

Article

State of Charge Estimation for Power Battery Using Improved Extended Kalman Filter Method Based on Neural Network

Xiaoyu Liu ^{1,*}  and Xiang Zhang ²

¹ National Center for Applied Mathematics in Chongqing, Chongqing Normal University, Chongqing 401331, China

² School of Mathematical Sciences, Chongqing Normal University, Chongqing 401331, China; zhxiang1012@163.com

* Correspondence: xyliu@cqnu.edu.cn

Abstract: In order to enhance the accuracy of the traditional extended Kalman filter (EKF) algorithm in the estimation of the state of charge (SoC) of power batteries, we first derived the state space equation and measurement equation of lithium power batteries based on the Thevenin battery model and the modified Ampere-Hour integral algorithm. Then, the basic principles of EKF, backpropagation neural networks (BPNNs), and a biogeography-based optimization (BBO) algorithm were analyzed, and the arc curve mobility model was used to improve the global search ability of the BBO algorithm. By combining these three algorithms, this paper proposes a BP neural network method based on the BBO algorithm. This method uses the BBO algorithm to optimize the incipient weight and threshold of the BP neural network and uses this improved neural network to modify the estimated value of the extended Kalman filter algorithm (BBOBP-EKF). Finally, the BBOBP-EKF algorithm, the extended Kalman filter algorithm based on the BP neural network (BP-EKF), and the EKF algorithm are used to estimate the error value of the SOC of a power battery, and according to the experimental data, it was confirmed that the proposed BBOBP-EKF algorithm has been improved compared to other algorithms with respect to each error index term, in which the maximum error is 1% less than that of the BP-EKF algorithm and 2.4% less than that of the EKF algorithm, the minimum error is also the smallest, and the estimation accuracy is improved compared to the traditional algorithms.

Keywords: extended Kalman filter algorithm; biogeography-based optimization algorithm; BP neural network; state of charge estimate



Citation: Liu, X.; Zhang, X. State of Charge Estimation for Power Battery Using Improved Extended Kalman Filter Method Based on Neural Network. *Appl. Sci.* **2023**, *13*, 10547. <https://doi.org/10.3390/app131810547>

Academic Editor: Andreas Sumpster

Received: 15 August 2023

Revised: 15 September 2023

Accepted: 18 September 2023

Published: 21 September 2023



Copyright: © 2023 by the authors. Licensee MDPI, Basel, Switzerland. This article is an open access article distributed under the terms and conditions of the Creative Commons Attribution (CC BY) license (<https://creativecommons.org/licenses/by/4.0/>).

1. Introduction

The recent problems with energy and the degradation of the environment have posed significant difficulties for individuals. The current rapid development of electric vehicles (EVs) not only effectively reduces the pressure on oil resources but also reduces the harm noise and air pollution inflict on people. As the key component of an electric vehicle, a power battery is not only the energy source of an electric vehicle but also an important energy storage device, which enormously influences the safety as well as performance of electric vehicles. In accordance with formula (1), the state of charge (SoC) of a power battery is the proportion between the battery's remaining capacity and its maximum capacity under certain conditions. Accurate battery estimates are a vital factor in ensuring battery performance, enhancing service safety and extending service life according to the SoC [1,2].

$$SoC = \frac{Q_t}{Q} \times 100\% \quad (1)$$

In the equation above, Q_t denotes the capacity of a battery at time t , and Q denotes a battery's maximum capacity.

Based on relevant investigations, a variety of methods are frequently employed to estimate the SoC of power batteries. Some of these methods include the Ampere-Hour

integral method [3], the open circuit voltage (OCV) method [4], the model-based Kalman filter (KF) [5], and data-based neural networks [6]. Regarding the estimation of SoC, there is a cumulative error in the open-circuit voltage method, and the Ampere-Hour integral method cannot make estimates in real time. The model-based Kalman filter [7] is an optimal recursive estimation method for dynamic linear system state estimation. It is a recursive predictive filtering algorithm. This method has good path-tracking performance and high accuracy. It is an effective online SoC estimation method [8], but the observation equation required by this method must be linear. To solve the optimal estimation problem in nonlinear systems, scholars have proposed an extended Kalman filter (EKF) [9] algorithm for nonlinear system models. Plett [10–12] first proposed a series of EKF-based SoC estimation algorithms for electric vehicle power batteries, which laid a theoretical foundation for the development of the EKF algorithm. However, the EKF algorithm linearizes nonlinear systems through Taylor series expansion, omits the high-order term, and thus introduces high-order loss error. Lee et al. [13] implemented the dual extended Kalman filter (DEKF) in an electrochemical model and proposed a battery SoC estimation method based on OCV-SoC. The obtained simulation results showed that the model method had good accuracy, and the initial error was less than $\pm 5\%$. Mastali et al. [14] used EKF and DEKF methods to estimate the SoC of a LiFePO₄ battery under different state models, and the results showed that the maximum error of the estimated SoC was 4%. Xiong et al. [15,16] proposed an online estimation method of battery open circuit voltage using an adaptive extended Kalman filter (AEKF) and evaluated four different types of lithium batteries' (LiB) SoC according to the improved Thevenin model and the OCV-SoC relationship. This method reduces the SoC estimation error by 4%. With the rapid development of the field of machine learning, the authors of [17] obtained battery parameters such as current, voltage, and temperature through experiments and used the improved backpropagation neural network (BPNN) to estimate the SoC value of a battery. In order to further improve the SoC estimation accuracy of power batteries, the researchers combined a data-based neural network with a filtering algorithm to compensate for the inaccuracy of the model and the complexity of calculation. The authors of [18,19] used a BP neural network to compensate for the error caused by the EKF linearization process to optimize SoC estimation accuracy. Although BP neural networks have the advantages of a simple structure, strong parameter adjustability, and high reliability, the uncertainty of the initial weights and thresholds of these networks makes their convergence speed slow and easily prone to falling into a local minimum. For this reason, we selected an intelligent algorithm, biogeography-based optimization (BBO) [20], which is simple in structure and easy to implement. This algorithm is a good complement to a BP neural network. At the same time, we also improved the traditional linear mobility model of this algorithm and introduced a nonlinear mobility model to improve the global search ability and adaptability of this algorithm. The improved BBO algorithm is used to optimize the initial weight and threshold of a BP neural network, and the optimized BP neural network is used to modify the SoC estimation value predicted by the EKF algorithm so as to obtain a more accurate SoC estimation value than the traditional algorithm. Numerical examples are used to verify the performance of the proposed BBOBP-EKF algorithm. The experimental results show that the error result of this algorithm is significantly improved compared with that of the EKF algorithm, and it is also improved compared with that of the BP-EKF algorithm.

2. Battery State Space Model

The EKF algorithm is used to estimate the dynamic SoC of a battery. A nonlinear observer is often combined with a battery model. The selection of a battery model has an important impact on obtaining an accurate SoC value. The common SoC estimation models include the electrochemical model (EM), the electrochemical impedance model (EIM), and the equivalent circuit model (ECM). It must be considered that it is difficult for the electrochemical model to determine all parameters, and the corresponding calculation is complex and time consuming [21], while the electrochemical impedance model is difficult,

complex, and limited in terms of the actual matching process [22]. The equivalent circuit model can more accurately describe the dynamic behavior of a battery, and it is easy to implement and readily improves the accuracy in SoC estimation. For the Rint model [23], Thevenin model [15], and the second-order resistance capacitance parallel model [24] in the equivalent circuit model, fully considering the complexity and accuracy of the model, the commonly used Thevenin equivalent circuit model with a first-order RC circuit was selected to establish the battery state space model, as Figure 1 illustrates.

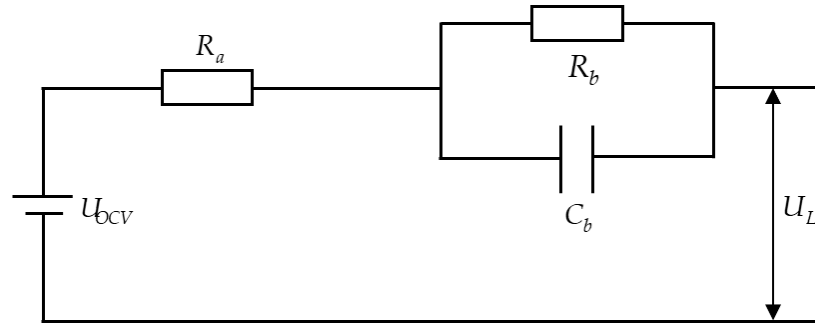


Figure 1. Thevenin battery model.

Based on the Thevenin equivalent battery model, and according to Kirchoff’s law, the continuous state space equation of the battery is obtained, that is, the voltage and current are as follows (2) [25]:

$$\begin{cases} U_L(t) = U_{OCV}(t) - U_b(t) - I(t) \cdot R_a(t) \\ I(t) = \frac{U_b(t)}{R_b} + C_b \cdot \frac{d(U_b(t))}{dt} \end{cases} \quad (2)$$

In the formula, $U_L(t)$ represents the output voltage at time t ; $U_{OCV}(t)$ is the battery open circuit voltage at time t , which is a nonlinear function varying with SoC; $U_b(t)$ represents the voltage of the RC circuit at time t ; R_a, R_b , and C_b represent the internal resistance of the battery, the resistance of the battery circuit, and the capacitance of the battery circuit, respectively; $I(t)$ represents the total charging and discharging current at time t .

From Equation (2), the discrete state space Equation (3) [25] can be derived

$$\begin{cases} U_b(k) = U_b(k-1) \cdot e^{-\frac{\Delta t}{R_b C_b}} + I(k-1) \cdot R_b (1 - e^{-\frac{\Delta t}{R_b C_b}}) \\ U_L(k) = U_{OCV}(k) - I(k) \cdot R_a - U_b(k) \end{cases} \quad (3)$$

where Δt is the sampling interval time, which is usually 1. k represents the number of sampling times. Then, the SoC value of lithium battery can be estimated using a modified Ampere-Hour integral method [26].

$$SoC(t) = SoC(0) - \frac{\int_0^t T_k \eta I dt}{Q} \quad (4)$$

where η is the charging and discharging efficiency of the battery, T_k is the temperature correction factor, and Q indicates the rated capacity of the battery. They are all definite values in the numerical experiments. The discretization of Equation (4) [26] can be obtained as follows:

$$SoC(k+1) = SoC(k) - \frac{T_k \eta \Delta t}{Q} I(k) \quad (5)$$

To sum up, the equation expression of the model’s state space can be deduced, which can be seen in Equation (6):

$$\begin{cases} \begin{bmatrix} SoC(k) \\ U_b(k) \end{bmatrix} = \begin{bmatrix} 1 & 0 \\ 0 & e^{-\frac{\Delta t}{R_b C_b}} \end{bmatrix} \begin{bmatrix} SoC(k-1) \\ U_b(k-1) \end{bmatrix} + \begin{bmatrix} -\frac{T_k \eta \Delta t}{Q} \\ R_b(1 - e^{-\frac{\Delta t}{R_b C_b}}) \end{bmatrix} I(k-1) + \boldsymbol{w}(k-1) \\ U_L(k) = U_{OCV}(k) - U_b(k) - R_a I(k) + v(k) \end{cases} \quad (6)$$

In the equation, $\boldsymbol{w}(k), v(k)$ represents the process noise and observation noise of the system at time k , and the corresponding variances are \boldsymbol{q}_k and r_k , respectively.

In this paper, 18,650 individual lithium-ion power batteries are used. Because the temperature will have a certain impact on the activity of the reactants inside the battery, excessively low activity will reduce the battery’s capacity, and excessively high activity will damage the battery, so the experiment was carried out at a constant temperature of 25 °C. The battery tester used was a Xinwei BTS-5V6A charge–discharge tester. During the experiment, the SoC and OCV values of charge and discharge were calibrated many times at the same time, and the mean values of these values were calculated [27]. It was necessary to perform a few criteria charging and discharging operations on the tester: according to the results of the experiment, a group of open-circuit voltage and state-of-charge records of average charge and discharge were ultimately gained, and the data were fitted using the least-squares method. The fourth-order fitting expression is presented in Equation (7) for further details, and the OCV-SoC fitting curve is shown in Figure 2.

$$U_{OCV} = -10.3263SoC^4 + 22.4018SoC^3 - 16.3058SoC^2 + 5.0034SoC + 3.2026 \quad (7)$$

where U_{OCV} stands for the battery’s open-circuit voltage.

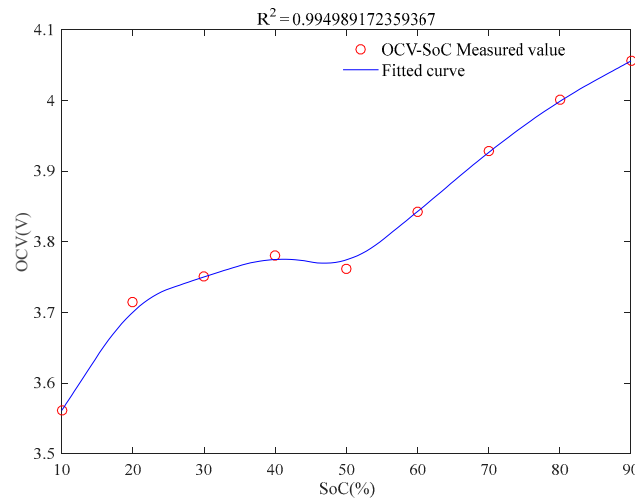


Figure 2. OCV-SoC fitting curve of battery.

3. Algorithm Design

3.1. EKF Algorithm

The classical Kalman filter is an optimal recursive estimation prediction method widely used in dynamic linear system state estimation. In the actual operation of an electric vehicle’s lithium battery, the system is highly nonlinear, and the extended Kalman filter algorithm can linearize this nonlinear system so as to estimate the battery’s SoC. The filtering algorithm involves two steps: prediction and correction. Equation (6) has been derived from the Thevenin battery equivalent model. In order to facilitate the operation of the algorithm later, the nonlinear system model (Equation (8)) is obtained by rewriting Equation (6) in compact form

$$\begin{cases} \boldsymbol{x}_k = f(\boldsymbol{x}_{k-1}, I_{k-1}) + \boldsymbol{w}_{k-1} \\ z_k = h(\boldsymbol{x}_k, I_k) + v_k \end{cases} \quad (8)$$

where $f(\cdot)$ and $h(\cdot)$ represent the state function and observation function of the system, respectively, and are the inputs of the system at a given time. From Equation (6), we can obtain $x_k = [SoC(k), U_b(k)]^T$, $w_{k-1} = w(k-1) = [w_1(k-1), w_2(k-1)]^T$, and $z_k = U_L(k)$, $v_k = v(k)$.

In order to facilitate further research on the EKF algorithm, Equation (2) can be used to create the state transition matrix of system **A**, noise matrix **B**, and observation matrix **C**, as shown in Equation (9) [25]. See Figure 3 for a specific flow chart of the EKF algorithm.

$$A = \begin{bmatrix} 1 & 0 \\ 0 & e^{-\frac{\Delta t}{R_b C_b}} \end{bmatrix}, B = \begin{bmatrix} -\frac{T_k \eta \Delta t}{Q} \\ R_b (1 - e^{-\frac{\Delta t}{R_b C_b}}) \end{bmatrix}, C_k = \frac{\partial h}{\partial x} \Big|_{x=x_k} = \left[\frac{dU_{OCV}}{dSoC} \Big|_{SoC=SoC(k)} \quad -1 \right] \tag{9}$$

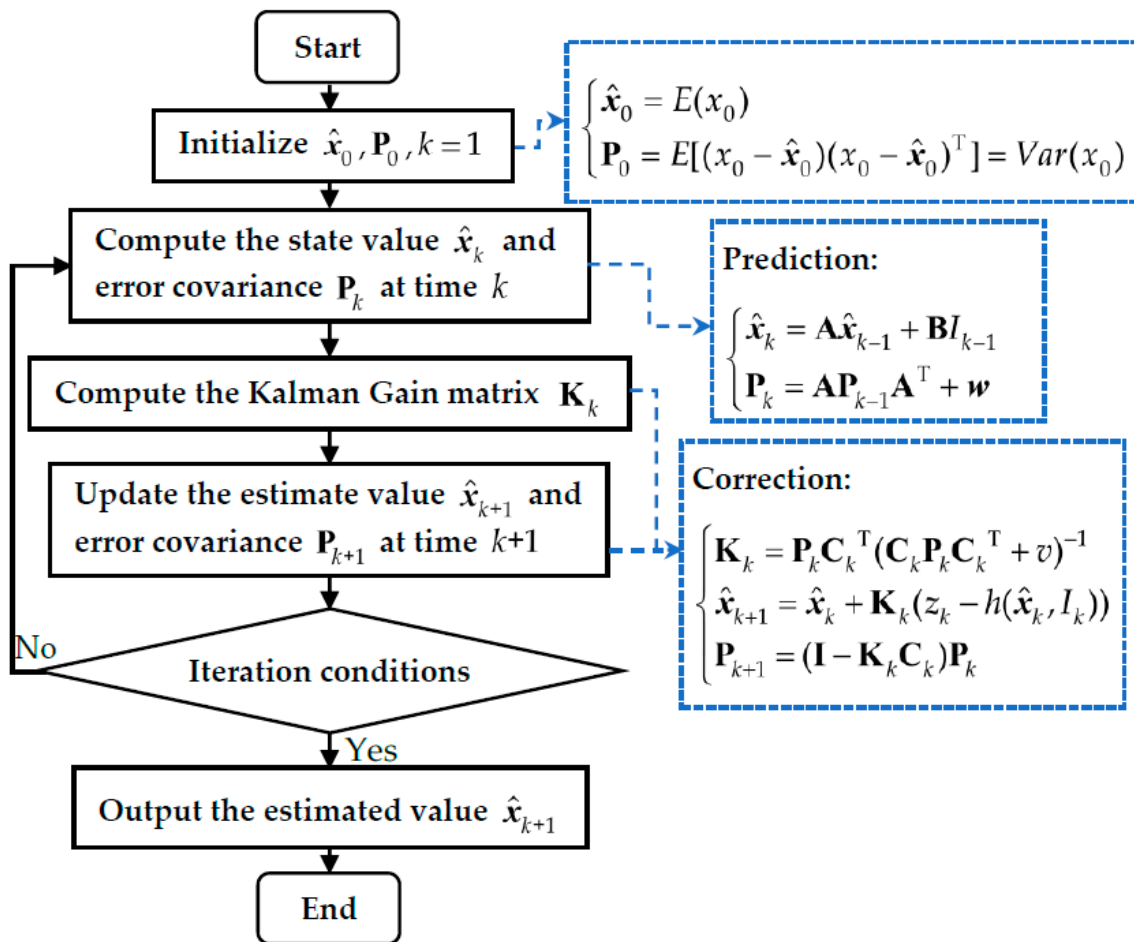


Figure 3. EKF algorithm flowchart.

3.2. BP Neural Network

The BP neural network is the first and foremost network put forward by Rumelhart and McClelland. It is an error-backpropagation-based multi-layer feed-forward neural network training model. It has a broad range of nonlinear input–output mode-mapping interactions that it can learn [28]. During the training process, taking the error as a sample, it constantly adjusts the weight and threshold between each layer so as to make the error meet the requirements [29]. Its neural network framework consists of an input layer, a hidden layer, and an output layer. In the course of estimating a battery’s SoC using the EKF algorithm, the SoC estimation results will produce errors due to various external factors. In order to compensate for this error, the BP neural network is introduced to compensate for and optimize the estimated value of the EKF.

3.2.1. Data Sources and Pretreatment

Regarding the data sources and pretreatment, firstly, the current, voltage, and temperature of the battery were collected through experiments and used as the basic data. Then, they were incorporated into the model expression to obtain the input data of the BP neural network using the EKF algorithm. For the sake of reducing the influence of singular sample data on the neural network, the input and output parameters need to be normalized through Equation (10), that is, the data must be processed into decimals between $[-1, 1]$, and the predicted data also need to be denormalized. For the input and output data, q ,

$$q' = 2 \times \frac{q - q_{min}}{q_{max} - q_{min}} - 1 \tag{10}$$

where q' is the normalized value, and the input and output data's minimum and maximum amounts are q_{min} and q_{max} , respectively.

3.2.2. Structure Design of BP Neural Network

The current study establishes one hidden layer in a BP neural network structure. Each time the SoC value is estimated, the battery temperature T at time $k + 1$, the Kalman gain matrix \mathbf{P}_k , and the SoC state value difference $\Delta\hat{x}_{k+1} (= \hat{x}_{k+1} - \hat{x}_k)$ estimated via the EKF algorithm at time k and time $k + 1$ are input into the trained neural network model, and the SoC estimation error ΔSoC_{k+1} is taken as the output to remove the estimation error ΔSoC_{k+1} from the estimated value \hat{x}_{k+1} . Finally, the estimated value SoC_{k+1} of the SoC quantity of a state at time $k + 1$, namely, $SoC_{k+1} = \hat{x}_{k+1} + \Delta SoC_{k+1}$, is obtained (see Figure 4 below).

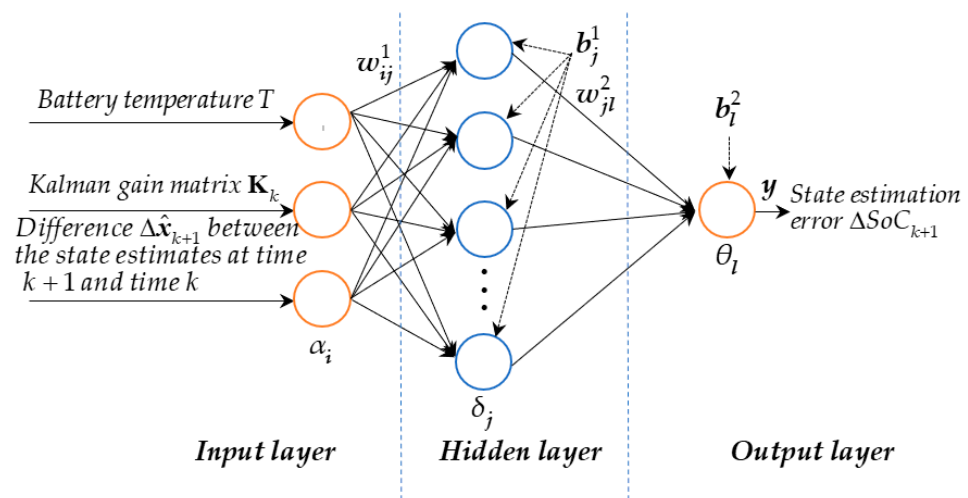


Figure 4. Specific structure and parameter diagram of BP neural network.

Let m , n , and s in Figure 4 equal the quantity of nodes in the input layer, hidden layer, and output layer; i , j , and l denote the input layer, hidden layer, and output layer, with i , j , and l neurons in each case. In this paper, the number of input layer nodes is $m = 3$, the quantity of output nodes is $s = 1$, and the quantity of hidden layers of the BP neural network may be determined via a trial-and-error method; the common formula is $n = \sqrt{m + s} + a$ (where a is the constant within the range from 1 to 10) [30]. After many simulation tests, when the quantity of hidden layer nodes is $n = 7$, the network prediction accuracy is higher, and the convergence speed is faster. w_{ij}^1 and w_{jl}^2 denote the weights that travel from the i -th input layer node to the j -th hidden layer node in addition to the j -th hidden layer node to the l -th output layer node in the network, respectively. The j -th nodes across the network in the hidden layer contain a threshold of b_j^1 ; meanwhile, the l -th nodes across the network in the output layer have a threshold of b_l^2 .

According to the quantity of nodes in each layer determined in this paper, from the input layer to the hidden layer, the weight matrix equals \mathbf{W}^1 , and the threshold matrix equals \mathbf{B}^1 . The weight matrix from the hidden layer to the output layer equals \mathbf{W}^2 , and the threshold matrix equals \mathbf{B}^2 . The input vector equals \mathbf{X} , the output vector equals \mathbf{Y} , the expected output vector equals \mathbf{O} , the hidden layer output value vector equals \mathbf{V} , the hidden layer error value vector equals \mathbf{U}^1 , and the output layer error value matrix equals \mathbf{U}^2 , as shown in Equations (11) and (12)

$$\mathbf{W}^1 = \begin{bmatrix} w_{11}^1 & w_{12}^1 & \cdots & w_{17}^1 \\ w_{21}^1 & w_{22}^1 & \cdots & w_{2n}^1 \\ w_{31}^1 & w_{32}^1 & \cdots & w_{37}^1 \end{bmatrix}, \mathbf{B}^1 = \begin{bmatrix} b_1^1 \\ b_2^1 \\ \vdots \\ b_7^1 \end{bmatrix}, \mathbf{W}^2 = \begin{bmatrix} w_{11}^2 \\ w_{21}^2 \\ w_{71}^2 \end{bmatrix}, \mathbf{B}^2 = [b_1^2] \quad (11)$$

$$\mathbf{X} = \begin{bmatrix} \alpha_1 \\ \alpha_2 \\ \alpha_3 \end{bmatrix} = \begin{bmatrix} T \\ \mathbf{K}_k \\ \Delta \hat{x}_{k+1} \end{bmatrix}, \mathbf{Y} = [\theta_1] = y, \mathbf{O} = [o_1], \mathbf{V} = \begin{bmatrix} \delta_1 \\ \delta_2 \\ \vdots \\ \delta_7 \end{bmatrix}, \mathbf{U}^1 = \begin{bmatrix} u_1^1 \\ u_2^1 \\ \vdots \\ u_7^1 \end{bmatrix}, \mathbf{U}^2 = [u_1^2] \quad (12)$$

where we also obtain $\mathbf{V} = g_1(\mathbf{W}^1 \mathbf{X} + \mathbf{B}^1)$ and $\mathbf{Y} = g_2(\mathbf{W}^2 \mathbf{V} + \mathbf{B}^2)$. The activation functions for the hidden layer and the output layer in each case are $g_1(\cdot)$ and $g_2(\cdot)$, and the two activation functions can be the same.

The objective function of the BP neural network training is shown in Equation (13)

$$F = \frac{1}{S} \sum_{\lambda=1}^S (y_1^\lambda - o_1^\lambda)^2 \quad (13)$$

where S is the quantity of training samples, the quantity of output layer nodes is 1, o_1^λ is the expected output value of the output node of sample λ , and y_1^λ is the actual output value of the output node under the action of sample λ .

3.3. Combination of BP Neural Network Optimized by BBO Algorithm and EKF

3.3.1. BBO Algorithm

In an attempt to imitate the migratory behavior of biological groups in nature, Simon [20] originally put forward a biogeography optimization method in 2008, which was centered on the migration operation of a linear model. The algorithm is uncomplicated in principle, easy to implement, contains fewer parameters, and has good global search capability and robustness. It is extensively applied in engineering [20,31,32], data analysis [33], and image processing [34]. The BBO algorithm mainly realizes the exchange of information through species migration and mutation between habitats. It then calculates the fitness value after exchange, and finally searches for the optimal solution through continuous iteration. Because the BP neural network is prone to falling into a local optimal solution in the training process, the application of the BBO algorithm to optimize the initial weight and threshold of a BP neural network can solve this problem to a certain extent, which helps to improve the optimization performance of a BP neural network and increase the number of opportunities to find a global optimal solution.

Because the core of the BBO algorithm is a migration operation, the traditional BBO algorithm is a linear mobility model (LMM) (see expression (14)), which has shortcomings in terms of its global search ability. This paper proposes a nonlinear mobility model, the arc curve mobility model (ACMM), as shown in expression (15), which advances the global search ability of the BBO algorithm.

$$\begin{cases} \lambda_n = I(1 - \frac{n}{m}) \\ \mu_n = E \cdot \frac{n}{m} \end{cases} \quad (14)$$

$$\begin{cases} \lambda_n = \begin{cases} \frac{I}{2} + \sqrt{\left(\frac{I}{2}\right)^2 - \left(\frac{n}{m}\right)^2}, & 0 \leq n < \frac{m}{2} \\ \frac{I}{2} - \sqrt{\left(\frac{I}{2}\right)^2 - \left(\frac{n}{m} - 1\right)^2}, & \frac{m}{2} \leq n \leq m \end{cases} \\ \mu_n = \begin{cases} \frac{E}{2} - \sqrt{\left(\frac{E}{2}\right)^2 - \left(\frac{n}{m}\right)^2}, & 0 \leq n < \frac{m}{2} \\ \frac{E}{2} + \sqrt{\left(\frac{E}{2}\right)^2 - \left(\frac{n}{m} - 1\right)^2}, & \frac{m}{2} \leq n \leq m \end{cases} \end{cases} \quad (15)$$

Above, λ_n and μ_n are the immigration rate and emigration rate when the quantity of biological populations in the current habitat is n , and their respective maximum values are equal to I and E . m is the maximum quantity of biological populations that the habitat can accommodate.

When the maximum quantity of biological populations $m = 50$, $I = 1$ and $E = 1$, as shown in Figure 5, can be obtained. It can be observed from the above expression or figure that the immigration rate λ and emigration rate μ will change with the change in the quantity of species n . When there are few species in the ecosystem, the circular arc curve mobility model can increase the immigration rate and slow decline, and the emigration rate will become small and slowly rise, which can increase the exchange of species information between habitats as well as boost the algorithm’s capacity for global search; when the quantity of species in the habitat is large, the immigration rate is small and the emigration rate is large, which also enhances the algorithm’s capacity for global search; when the quantity of species in the habitat is equal to half of the maximum quantity of species, the immigration rate is equal to the emigration rate, thus reaching a balance state. Please refer to Figures 5 and 6 for further information.

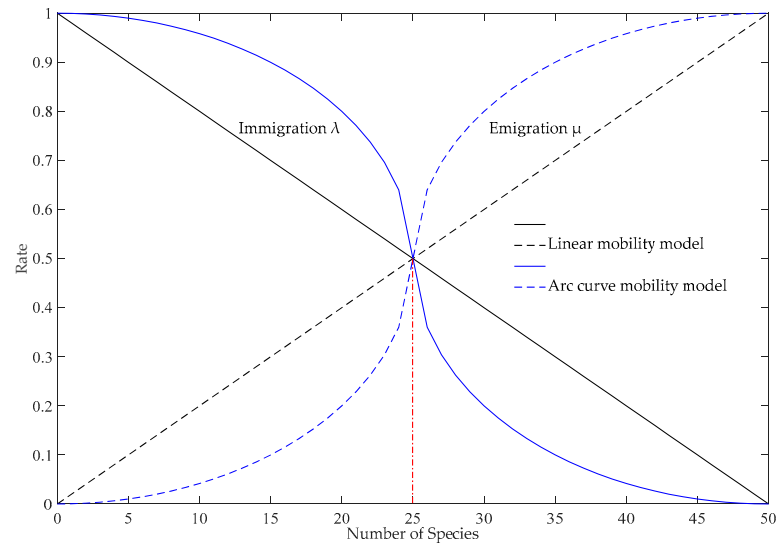


Figure 5. Linear/Arc curve mobility model diagram.

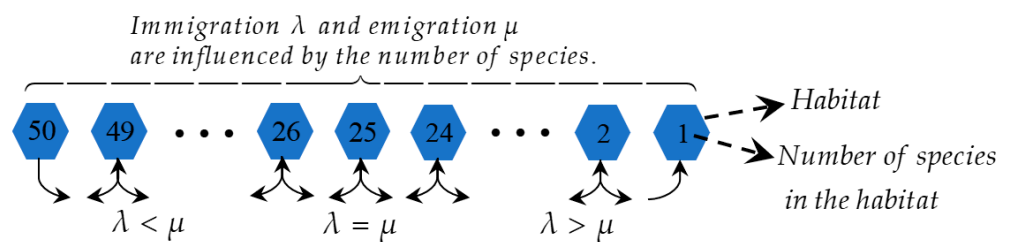


Figure 6. Species migration map for habitats and maximum species count of 50.

The habitat suitability index (HSI) is a metric utilized to assess whether an area is suitable for a species’ existence. The larger the value, the more suitable the habitat is for species survival. The HSI is composed of many factors, including temperature, rainfall,

vegetation and geological diversity, and land area. These factors affecting HSI are known as suitability index variables (SIV). Due to the limited resources of habitats, habitats with high suitability tend to accommodate more species, and local species are more likely to migrate to other habitats, while the immigration rate of alien species is low. However, habitats with low suitability tend to contain fewer species, and alien species are more likely to migrate to the local area and less likely to leave. In addition, large change events such as natural disasters may also change the state of habitats, thereby affecting the HSI.

3.3.2. Implementation Process of BBOBP-EKF Algorithm

The BBO algorithm is coupled with a BP neural network and applied to the correction of the estimated value of the EKF algorithm. Figure 7 shows the concrete implementation process diagram of the BBOBP-EKF algorithm. The specific method of SoC estimation is as follows: firstly, the EKF algorithm is used to estimate the SoC and calculate the input of the BP neural network, that is, the Kalman gain matrix P_k and the SoC state value difference $\Delta\hat{x}_{k+1} (= \hat{x}_{k+1} - \hat{x}_k)$ estimated by the EKF algorithm at time k and time $k + 1$ are used as two inputs of the network. As the temperature has a certain impact on the battery, the battery temperature T is also one of the inputs. Then, based on the neural network structure, the BBO algorithm is used to optimize the initial weight and threshold of the BP neural network, and the optimized weight and threshold are assigned to the neural network. Then, the network is trained and tested, and the SoC estimation error is output after meeting the conditions, which is the compensation value of the EKF algorithm's estimation error. Finally, the SoC value estimated using the EKF method is added to the compensation value output by the BP neural network to obtain the final SoC estimation value.

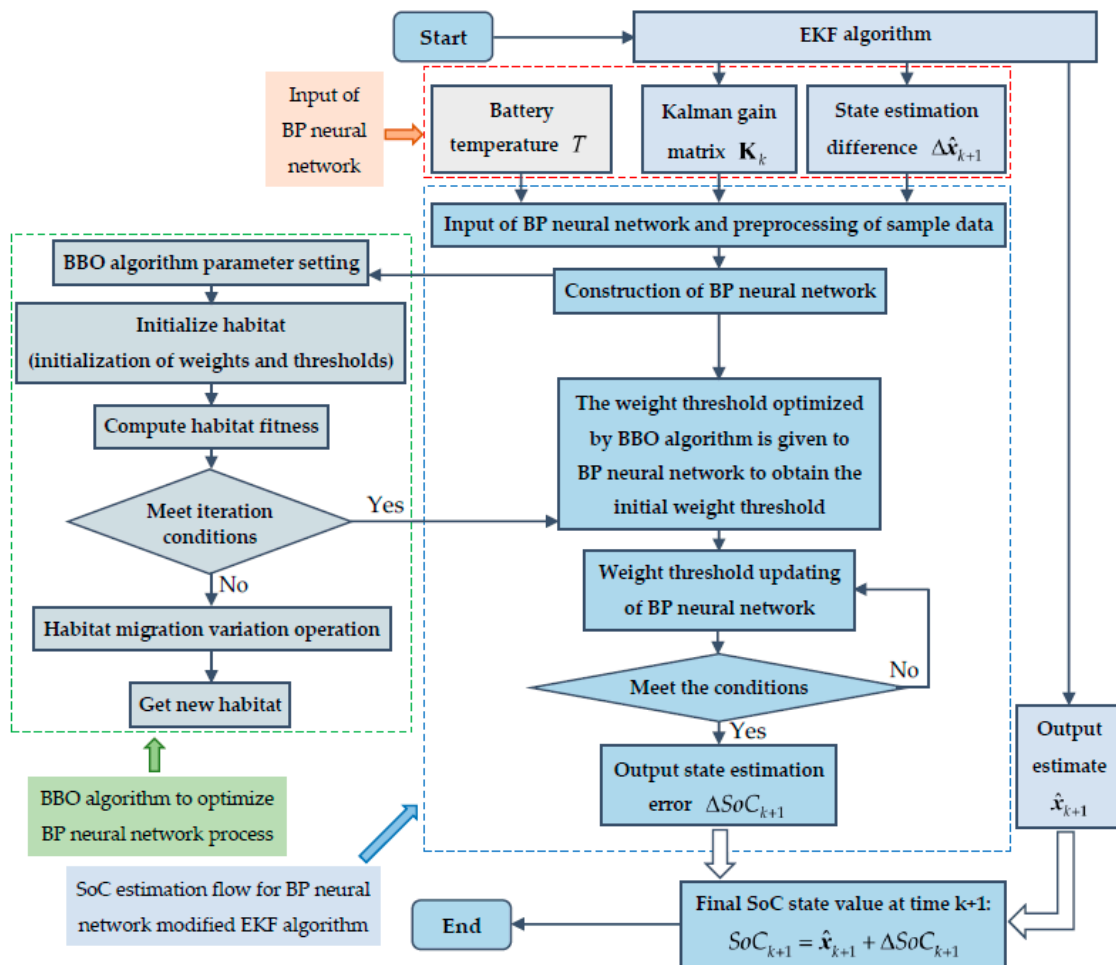


Figure 7. BBOBP-EKF algorithm estimation of battery SoC flowchart.

4. Experimental Results and Analysis

The experimental results were obtained using MATLAB simulation software (<https://ww2.mathworks.cn/discovery/simulation-software.html>). First, the SoC was estimated via the EKF algorithm, which is depicted in Figure 3. The current, voltage, and temperature data used were measured using the experimental equipment. The initial SoC value was set to 90%, the time step was 1 s, and the total simulation time was 2000 s, where $R_a = R_b = 15$, and $\tau = R_b C_b$ are time constants, which are generated by the normrnd function. The normal distribution generated by the randn function was used as the initial value of noise and observation noise, and the identity matrix generated by the eye function was used as the initial value of the covariance matrix.

Further, the BBO algorithm was used to optimize the weight and threshold of the BP neural network, and then the SoC estimation compensation value was output. Combined with the estimation value obtained using the EKF method, the SoC estimation value was finally obtained. By using the newff function to establish a forward-type BP neural network, experiments were conducted on 1000 sets of data, and the predicted output of the network was set to 1×10^{-5} . After 2000 iterations, the network was trained. As a training set, the first 900 collections of data were employed, while the last 100 groups of data served as the test set. The learning rate was 0.01, and the training goal error was 1×10^{-7} . The main parameter-setting steps of the BBO algorithm include setting the weight and threshold value range to $[-3, 3]$, the maximum quantity of iterations to 100, the quantity of habitats to 50, the habitat retention rate to 0.2, and the maximum mutation rate to 0.01. The following is a comparison of the results regarding the accuracy of the three algorithms for estimating lithium battery SoC value obtained through simulation, as shown in Figure 8.

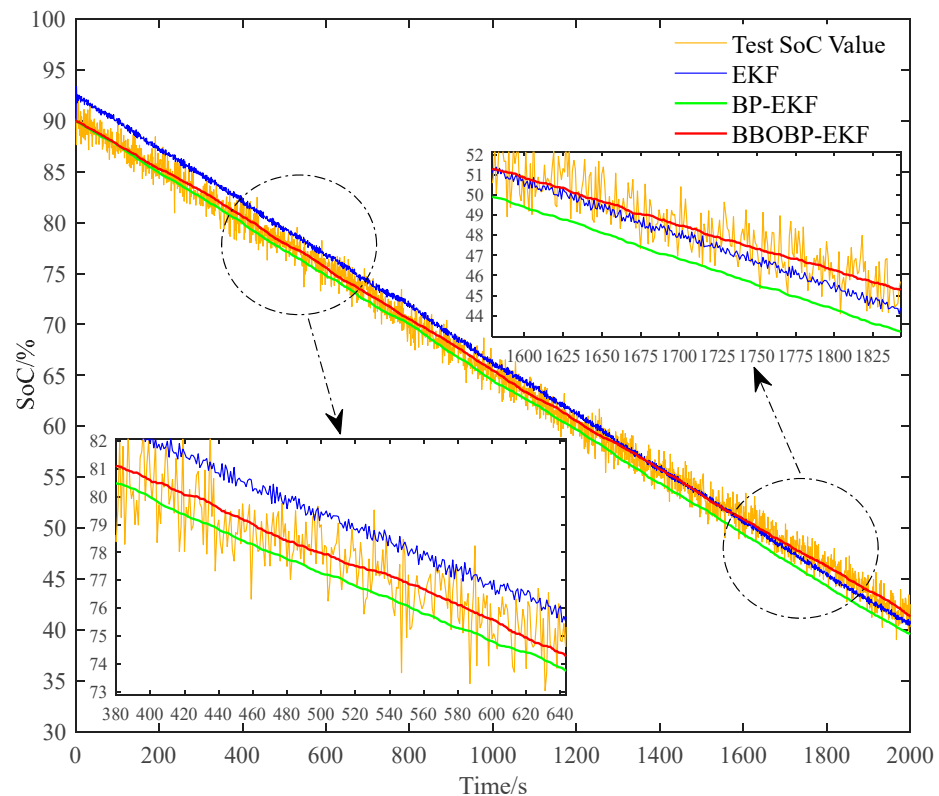


Figure 8. Comparison of SoC accuracy.

As can be seen in Figure 8, with the increase in simulation time, the experimental real value of the SoC of the power battery decreases, and the experimental measured value of the SoC fluctuates in an interval due to the addition of noise perturbation to the experiments, while the SoC value estimated via the BBOBP-EKF method is essentially in the middle of the interval of the experimental value and is very stable and fluctuates with the

fluctuation of the real SoC value, which is closer to the actual battery SoC value compared to the SoC value estimated by the BP-EKF algorithm and the EKF algorithm. Compared with the BP-EKF algorithm and the EKF algorithm, the estimated SoC values are closer to the actual battery SoC values, leading to the conclusion that the accuracy of the SoC values obtained via the BBOBP-EKF method has been improved to a certain extent. Meanwhile, after simulation, a comparison of the error curves of the EKF algorithm, BP-EKF algorithm, and BBOBP-EKF algorithm with respect to estimating the battery SoC value is also shown in Figure 9, which shows that the EKF algorithm fluctuates outside the error 0 value, and the BP-EKF algorithm and BBOBP-EKF method essentially fluctuate above and below the error 0 value, but the error float of the BBOBP-EKF method is much higher than that of the BP-EKF algorithm or the EKF algorithm; however, the error fluctuation of the BBOBP-EKF method is lower and more stable than that of the BP-EKF algorithm, so the BBOBP-EKF method is more effective in the estimation of battery SoC.

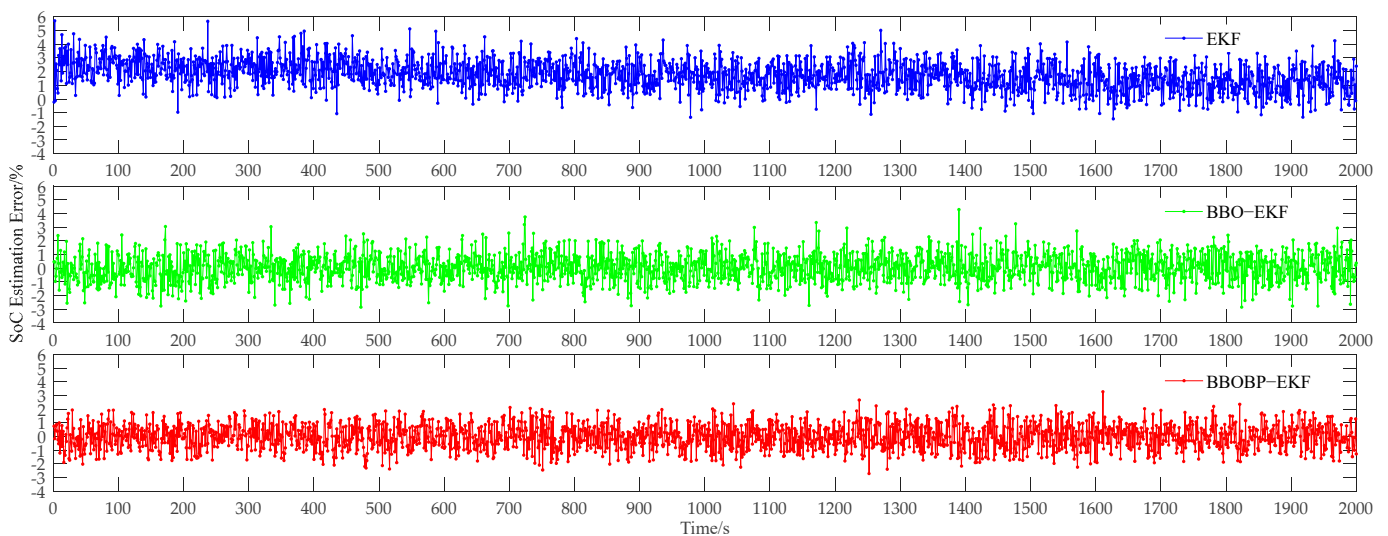


Figure 9. Comparison of different algorithms' errors.

For the purpose of the better characterization of the error values of different algorithms, the error values obtained by each algorithm are taken as absolute values, and the presented error values are shown in Figure 10. It may be deduced that the BBOBP-EKF approach has an absolute error value of 2000 times, which is basically within 2%. The error value corresponding to a number of times less than 1% is also higher than that of the other algorithms. Overall, it is superior to the BP-EKF algorithm and significantly better than the EKF algorithm. The number of times the error values obtained by different algorithms fall into different intervals is shown in Table 1.

Table 1. Comparison of the times of different algorithms in the absolute error range.

Error Taking Absolute Value Interval/%	EKF	BP-EKF	BBOBP-EKF
$0 \leq e \leq 1$	459	1331	1412 ¹
$1 < e \leq 2$	726	574	554
$2 < e$	815	95	34

¹ The values in digital boldface denote better performance compared to other algorithms in the table.

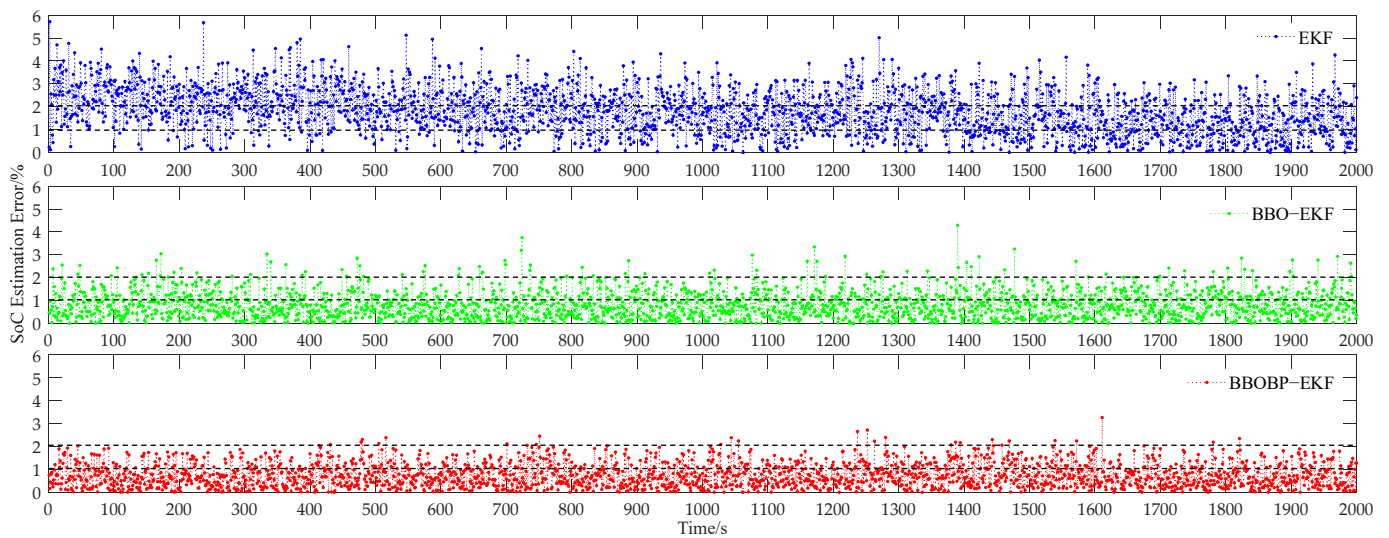


Figure 10. Comparison of absolute values of errors for different algorithms.

To further illustrate the effects of the three methods, the error results are shown in Table 2. The smaller the index of the SoC estimation error, the better the accuracy of the algorithm. Compared with the BP-EKF algorithm and EKF algorithm, the maximum error of the BBOBP-EKF algorithm is 1% less than that of the BP-EKF algorithm and 2.4% less than that of the EKF algorithm, and its minimum error is also the smallest. Furthermore, the smaller the variance of the error, the more stable the estimation method. The error index in Table 2 intuitively shows that the accuracy of battery SoC estimation based on the BBOBP-EKF method is slightly better than that of the BP-EKF algorithm and obviously better than that of the EKF algorithm.

Table 2. Comparison of error indicators of different algorithms.

Index	Minimum Error /%	Maximum Error /%	Mean Absolute Value of Error /%	Error Variance /%
EKF	1.6421×10^{-3}	5.7156	1.8099	1.1731
BP-EKF	9.9855×10^{-4}	4.2849	0.8207	1.0498
BBOBP-EKF	1.7112×10^{-4} ²	3.2658	0.7483	0.9443

² The values in digital boldface represent better performance compared to other algorithms in the table.

5. Conclusions

The lithium power battery space equation of state and the observed output equation were constructed in this study by utilizing the Thevenin cell model. Furthermore, the BBOBP-EKF method was developed to evaluate the SoC for batteries. The error of the EKF algorithm was corrected using a BP neural network, and the BBO method was adopted to improve the initial weights and thresholds of the BP neural network. In the end, the BBOBP-EKF method was compared with the BP-EKF algorithm and the EKF algorithm to obtain the SoC estimation error: the proposed method's maximum error was 1% lower than that of the BP-EKF algorithm and 2.4% lower than that of the EKF algorithm, and the minimum error was also reduced, thus demonstrating that the accuracy of battery SoC estimation founded on the BBOBP-EKF method was enhanced compared with that of other algorithms.

Author Contributions: Conceptualization, X.L. and X.Z.; methodology, X.L. and X.Z.; software, X.Z.; validation, X.Z.; formal analysis, X.Z.; investigation, X.L. and X.Z.; resources, X.L.; data curation, X.Z.; writing—original draft preparation, X.Z.; writing—review and editing, X.L. and X.Z.; visualization, X.L.; supervision, X.L. and X.Z.; project administration, X.L.; funding acquisition, X.L. All authors have read and agreed to the published version of the manuscript.

Funding: This work was supported by the key Science and Technology Research Program of Chongqing Municipal Education Commission [Grant No.KJQN202200543] and the Chongqing Municipal Graduate Research Innovation Project [CYS23414].

Institutional Review Board Statement: Not applicable.

Informed Consent Statement: Not applicable.

Data Availability Statement: Data are not disclosed due to confidentiality requirements.

Conflicts of Interest: The authors declare that they have no known competing financial interest or personal relationship that could have appeared to influence the work reported in this paper.

Abbreviations

EVs	Electric vehicles
SoC	State of charge
OCV	Open-circuit voltage
KF	Kalman filter
EKF	Extended Kalman filter
DEKF	Dual extended Kalman filter
AEKF	Adaptive extended Kalman filter
LiB	Lithium batteries
BPNN	Backpropagation neural network
BBO	Biogeography-based optimization
EM	Electrochemical model
EIM	Electrochemical impedance model
ECM	Equivalent circuit model
LMM	Linear mobility model
ACMM	Arc curve mobility model
HIS	Habitat suitability index
SIV	Suitability index variables

References

- Lu, L.; Han, X.; Li, J.; Hua, J.; Ouyang, M. A review on the key issues for lithium-ion battery management in electric vehicles. *J. Power Sources* **2013**, *226*, 272–288. [[CrossRef](#)]
- Hannan, M.A.; Lipu, M.S.H.; Hussain, A.; Mohamed, A. A review of lithium-ion battery state of charge estimation and management system in electric vehicle applications: Challenges and recommendations. *Renew. Sustain. Energy Rev.* **2017**, *78*, 834–854. [[CrossRef](#)]
- Lashway, C.R.; Mohammed, O.A. Adaptive battery management and parameter estimation through physics-based modeling and experimental verification. *IEEE Trans. Transp. Electrification* **2016**, *2*, 454–464. [[CrossRef](#)]
- Snihir, I.; Rey, W.; Verbitskiy, E.; Belfadhel-Ayeb, A.; Notten, P.H.L. Battery open-circuit voltage estimation by a method of statistical analysis. *J. Power Sources* **2006**, *159*, 1484–1487. [[CrossRef](#)]
- Afshar, S.; Morris, K.; Khajepour, A. State-of-charge estimation using an EKF-based adaptive observer. *IEEE Trans. Control Syst. Technol.* **2018**, *27*, 1907–1923. [[CrossRef](#)]
- Fasahat, M.; Manthouri, M. State of charge estimation of lithium-ion batteries using hybrid autoencoder and Long Short Term Memory neural networks. *J. Power Sources* **2020**, *469*, 228375. [[CrossRef](#)]
- Kalman, R.E. A new approach to linear filtering and prediction problems. *J. Basic Eng.* **1960**, *82*, 35–45. [[CrossRef](#)]
- Meng, J.; Ricco, M.; Luo, G.; Swierczynski, M.; Stroe, D.I.; Stroe, A.I.; Teodorescu, R. An overview and comparison of online implementable SoC estimation methods for lithium-ion battery. *IEEE Trans. Ind. Appl.* **2017**, *54*, 1583–1591. [[CrossRef](#)]
- Reif, K.; Unbehauen, R. The extended Kalman filter as an exponential observer for nonlinear systems. *IEEE Trans. Signal Process.* **1999**, *47*, 2324–2328. [[CrossRef](#)]
- Plett, G.L. Extended Kalman filtering for battery management systems of Li PB-based HEV battery packs: Part 1. Background. *J. Power Sources* **2004**, *134*, 252–261. [[CrossRef](#)]
- Plett, G.L. Extended Kalman filtering for battery management systems of Li PB-based HEV battery packs: Part 2. Modeling and identification. *J. Power Sources* **2004**, *134*, 262–276. [[CrossRef](#)]
- Plett, G.L. Extended Kalman filtering for battery management systems of Li PB-based HEV battery packs: Part 3. State and parameter estimation. *J. Power Sources* **2004**, *134*, 277–292. [[CrossRef](#)]
- Lee, S.J.; Kim, J.H.; Lee, J.M.; Cho, B. The State and Parameter Estimation of An Li-ion Battery Using A New OCV-SoC Concept. In Proceedings of the 2007 IEEE Power Electronics Specialists Conference, Orlando, FL, USA, 17–21 June 2007; pp. 2799–2803.

14. Mastali, M.; Vazquez-Arenas, J.; Fraser, R.; Fowler, M.; Afshar, S.; Stevens, M. Battery state of the charge estimation using Kalman filtering. *J. Power Sources* **2013**, *239*, 294–307. [[CrossRef](#)]
15. He, H.; Xiong, R.; Zhang, X.; Sun, F.; Fan, J. State-of-charge estimation of the lithium ion battery using an adaptive extended Kalman filter based on an improved Thevenin model. *IEEE Trans. Veh. Technol.* **2011**, *60*, 1461–1469.
16. Xiong, R.; Gong, X.; Mi, C.C.; Sun, F. A robust state-of-charge estimator for multiple types of lithium ion batteries using adaptive extended Kalman filter. *J. Power Sources* **2013**, *243*, 805–816. [[CrossRef](#)]
17. Hu, Y.; Wang, Z. Study on SoC Estimation of Lithium Battery Based on Improved BP Neural Network. In Proceedings of the 2019 8th International Symposium on Next Generation Electronics (ISNE), Zhengzhou, China, 9–10 October 2019; pp. 1–3.
18. Tian, D.; Li, L.; Yang, Y. Research on SoC estimation based on improved BP-EKF algorithm. *Chin. J. Power Sources* **2020**, *44*, 1274–1278.
19. Gao, Y.; Ji, W.; Zhao, X. SoC Estimation of E-Cell combining BP neural network and EKF algorithm. *Processes* **2022**, *10*, 1721. [[CrossRef](#)]
20. Simon, D. Biogeography-based optimization. *IEEE Trans. Evol. Comput.* **2008**, *12*, 702–713. [[CrossRef](#)]
21. Liu, G.; Lu, L.; Fu, H.; Hua, J.; Li, J.; Ouyang, M.; Wang, Y.; Xue, S.; Chen, P. A comparative study of equivalent circuit models and enhanced equivalent circuit models of lithium-ion batteries with different model structures. In Proceedings of the 2014 IEEE Conference and Expo Transportation Electrification Asia-Pacific (ITEC Asia-Pacific), Beijing, China, 31 August–3 September 2014; pp. 1–6.
22. Wang, Q.; He, Y.; Shen, J.; Hu, X. State of charge-dependent polynomial equivalent circuit modeling for electrochemical impedance spectroscopy of lithium-ion batteries. *IEEE Trans. Power Electron.* **2017**, *33*, 8449–8460. [[CrossRef](#)]
23. Nemes, R.; Ciornei, S.; Ruba, M.; Hedesiu, H.; Martis, C. Modeling and simulation of first-order Li-Ion battery cell with experimental validation. In Proceedings of the 2019 8th International Conference on Modern Power Systems (MPS), Cluj Napoca, Romania, 21–23 May 2019; pp. 1–6.
24. Zhang, X.; Lu, J.; Yuan, S.; Yang, J.; Zhou, X. A novel method for identification of lithium-ion battery equivalent circuit model parameters considering electrochemical properties. *J. Power Sources* **2017**, *345*, 21–29. [[CrossRef](#)]
25. Shi, Y.; Ahmad, S.; Tong, Q.; Lim, T.M.; Wei, Z.; Ji, D.; Eze, C.M.; Zhao, J. The optimization of state of charge and state of health estimation for lithium-ions battery using combined deep learning and Kalman filter methods. *Int. J. Energy Res.* **2021**, *45*, 11206–11230. [[CrossRef](#)]
26. He, Z.; Li, Y.; Sun, Y.; Zhao, S.; Lin, C.; Pan, C.; Wang, L. State-of-charge estimation of lithium ion batteries based on adaptive iterative extended Kalman filter. *J. Energy Storage* **2021**, *39*, 102593. [[CrossRef](#)]
27. Fan, B.; Ren, S.; Luo, J. Research on relationship between SoC and OCV of lithium ion battery under actual application conditions. *Chin. J. Power Sources* **2018**, *42*, 641–644.
28. McClelland, J.L.; Rumelhart, D.E.; PDP Research Group. *Parallel Distributed Processing*; MIT Press: Cambridge, MA, USA, 1986.
29. Ma, H.; Lipu, M.S.H.; Hussain, A.; Mohamad, H.S.; Afida, A. Neural network approach for estimating state of charge of lithium-ion battery using backtracking search algorithm. *IEEE Access* **2018**, *6*, 10069–10079.
30. Wang, S.; Ma, H.; Dou, J.; Zhang, Y.; Li, S.; Hu, L. Estimation of lithium-ion battery state of charge based on UGOA-BP. *Energy Storage Sci. Technol.* **2022**, *11*, 258–264.
31. Zhang, Y.; Gu, X. Biogeography-based optimization algorithm for large-scale multistage batch plant scheduling. *Expert Syst. Appl.* **2020**, *162*, 113776. [[CrossRef](#)]
32. Zhang, Z.; Gao, Y.; Zuo, W. A dual biogeography-based optimization algorithm for solving high-dimensional global optimization problems and engineering design problems. *IEEE Access* **2022**, *10*, 55988–56016. [[CrossRef](#)]
33. Xu, P.; Chen, S.; Yu, X.; Zhang, L. Developing a novel hybrid biogeography-based optimization algorithm for multilayer perceptron training under big data challenge. *Sci. Program.* **2018**, *2018*, 2943290.
34. Zhang, X.; Wen, S.; Wang, D. Multi-population biogeography-based optimization algorithm and its application to image segmentation. *Appl. Soft Comput.* **2022**, *124*, 109005. [[CrossRef](#)]

Disclaimer/Publisher’s Note: The statements, opinions and data contained in all publications are solely those of the individual author(s) and contributor(s) and not of MDPI and/or the editor(s). MDPI and/or the editor(s) disclaim responsibility for any injury to people or property resulting from any ideas, methods, instructions or products referred to in the content.